Computing Three-dimensional Constrained Delaunay Refinement Using the GPU

Zhenghai Chen and Tiow-Seng Tan
School of Computing
National University of Singapore
Singapore
{chenzh, tants}@comp.nus.edu.sg

***Abstract*—We propose the first GPU algorithm for the 3D constrained Delaunay refinement problem. For an input of a piecewise linear complex $\mathcal{G}$ and a constant B, it produces, by adding Steiner points, a constrained Delaunay triangulation conforming to $\mathcal{G}$ and containing tetrahedra mostly with radius-edge ratios smaller than B. Our implementation of the algorithm shows that it can be an order of magnitude faster than the best CPU software while using similar quantities of Steiner points to produce triangulations of comparable qualities. It thus reduces the computing time of triangulation refinement from possibly an hour to a few seconds or minutes for possible use in interactive applications.**

***Index Terms*—GPGPU, Computational Geometry, Mesh Refinement, Finite Element Analysis**

I. INTRODUCTION

Triangulations are used in various engineering and scientific applications such as finite element methods, interpolation etc. Such a triangulation, in general, is obtained from a so-called *piecewise linear complex* (PLC) $\mathcal{G}$ containing a point set P, an edge set E (where each edge has endpoints in P), and a polygon set F (where each polygon has boundary edges in E) [1]. Specifically, a *triangulation* $\mathcal{T}$ of $\mathcal{G}$ is a decomposition of the convex hull of P into tetrahedra where the intersection of any two tetrahedra is either empty, a vertex, an edge, or a triangle of both tetrahedra. In addition, all vertices, edges and polygons of $\mathcal{G}$ also appear in $\mathcal{T}$ as vertices, unions of edges, and unions of triangles, respectively; we also say $\mathcal{T}$ *conforms* to $\mathcal{G}$ in this case. To ease our discussion, we call an edge in E a *segment*, an edge in $\mathcal{T}$ which is also a part or whole of some segment a *subsegment*, and a triangle in $\mathcal{T}$ which is also a part or whole of some polygon in F a *subface*.

In a situation where the given PLC includes the watertight boundary of an object, such as the elephant in Figure 1(a), we are interested mainly in the part of the triangulation enclosed within the boundary instead of the convex hull of the vertices of the PLC.

As there are possibly many triangulations of a given $\mathcal{G}$, many applications prefer a so-called *constrained Delaunay triangulation* (CDT) with few *bad* tetrahedra. A CDT is a triangulation where each tetrahedron t in $\mathcal{T}$ is such that the circumsphere of t either encloses no vertices of $\mathcal{T}$ or only vertices of $\mathcal{T}$ that are invisible to any interior point of t (Figure 1(b) is a cut-off view of the CDT of Figure 1(a)). Two points are *invisible* to each other if the line segment joining them intersects any subface (not containing the line segment); otherwise, they are *visible*. For our purpose, a tetrahedron t is *bad* if the ratio of the radius of its circumsphere to its shortest edge, termed as *radius-edge ratio*, is larger than some predetermined constant B. [1]

For a given input B and a CDT $\mathcal{T}$ of $\mathcal{G}$, the constrained Delaunay refinement problem is to add vertices, called *Steiner points*, into $\mathcal{T}$ to eliminate most, if not all, bad tetrahedra to generate a new CDT of $\mathcal{G}$. A solution to the problem should also aim to add few Steiner points. Figure 1(c) shows (one in a cut-off view and one in a boundary view) a refinement of the triangulation in Figure 1(b) to one with few bad tetrahedra. The `TetGen` software by Si [3] is the best CPU solution known to the problem. It, however, can take a significant amount of time, from minutes to hours, to compute CDTs for some typical inputs from applications. We are thus interested to explore parallel computations to reduce the computing time of this problem. Two commonly accessible hardware for parallel computations are: multicore CPU and GPU. For the former, we learn in [4] that modern CPU with 64 cores, so far, is only able to achieve a single digit speedup for a simpler (non-constrained) triangulation refinement problem, and in [5], similar findings with older multicore machines. For the latter, the CDT refinement problem studied here is not known to present itself readily for a GPU computation, and we do not find any prior good solution in the past decade of GPU history.

The challenge to GPU computation is to design a balanced workload algorithm to have all working GPU threads having roughly the same amount of work to complete in the many rounds of computations, and in each round to be able to utilize the GPU resources well to deploy as many GPU threads as possible. At times, it is unavoidable that some GPU threads are bound to do work that do not contribute to the final answer, but such waste must be minimized to still achieve good speedup. To this end, we have addressed these challenges by developing the first working GPU solution for

Project webpage: https://www.comp.nus.edu.sg/~tants/gqm3d.html. The research is supported by the National University of Singapore under grant R-252-000-678-133.

[1]The radius-edge ratio has become a standard measure used for Delaunay refinement algorithms. Though a tetrahedron with a small radius-edge ratio and yet of a small volume, called *sliver*, is also not ideal for applications, it can be eliminated relatively easily in practice; see [2].

978-1-7281-3613-4/19/$31.00 ©2019 IEEE
DOI 10.1109/PACT.2019.00039

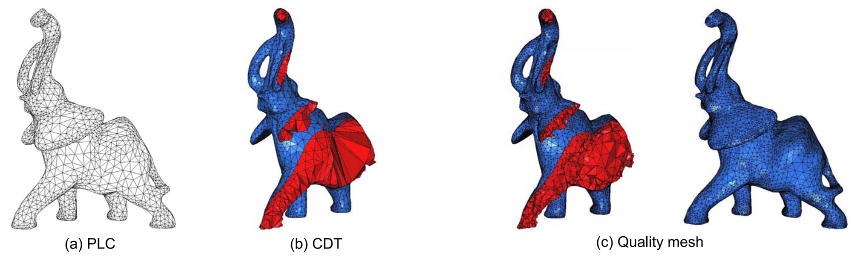

Fig. 1. gQM3D working on the PLC of an elephant.

the CDT refinement problem. Specifically, its contributions are as follows:

(1) a GPU algorithm, gQM3D, and a CPU-GPU hybrid variant, gQM3D$^+$, that solve the CDT refinement problem for PLC with an order of magnitude speedup as compared to the best CPU software, TetGen while still maintaining similar output sizes and comparable qualities;
(2) at the algorithmic level, an efficient and effective parallel GPU pipeline, InsertPoints, to concurrently insert points to refine a triangulation, which can be useful to solve other refinement problems; and
(3) at the data structure level, a *tuple* structure to keep track of work in progress and result of work done to provide good support for the extensive use of parallel prefix and stream compaction in the GPU solution.

In this paper, we start the discussion with Section II which reviews important previous work, and then Section III which discusses the considerations and challenges of designing our GPU solution, followed by Section IV which details the proposed algorithms gQM3D and gQM3D$^+$. Then, Section V presents our experimental results in comparison with the best CPU software, TetGen, and finally, Section VI concludes the paper.

II. Literature Review

In 2D, Chew [6], [7] and Ruppert [8] proposed algorithms that output triangulations whose triangles have good attributes (such as no small angles) for an input of points and segments. On the same problem, Chen *et al.* [9] developed a GPU algorithm that unifies both Chew's and Ruppert's to achieve good speedup of over an order of magnitude.

In 3D, Dey *et al.* [10] and Chew [11] generalized Chew's algorithm [7] to compute the Delaunay triangulation of a set of input points without constraints. Both algorithms produce uniform triangulations that contain tetrahedra of roughly the same size. However, they sometimes need many more tetrahedra than necessary as they do not take advantage of using different large size tetrahedra where possible. For an input of a constant B and a PLC, Shewchuk [2] proposed a provably correct Delaunay refinement algorithm. The algorithm is guaranteed to terminate with a conforming Delaunay triangulation when $B > 2$ and the PLC has no acute angles. However, this approach may need to use a large number of Steiner points to complete the computation.

An alternative approach is to first compute a CDT, as discussed in Shewchuk [12] and Si [13], and then further refine the CDT to one with few, if any, bad tetrahedra. This approach, as implemented by Si [3] in TetGen, usually produces a smaller triangulation than that of Shewchuk's algorithm [2] which generates the conforming Delaunay triangulation.

Oudot *et al.* [14] introduced a triangulation generation algorithm for input domains bounded by smooth surfaces while Cheng *et al.* [15] for piecewise smooth complexes. Both algorithms, as implemented in CGAL [16], use the notion of a restricted Delaunay triangulation to approximate the domain boundary by a new boundary triangulation. Because of this approximation, the output need not conform to the input surface or complex. Building on top of CGAL, Hu *et al.* [17] proposed an algorithm called TetWild that converts a triangle soup into a triangulation. This algorithm focuses on robustness and is often slower than both TetGen and CGAL.

In parallel computation, Blandford *et al.* [18] proposed a space-efficient Delaunay algorithm based on a concurrent compressed data structure, while Foteinos and Chrisochoides [5] presented one that offers fully dynamic parallel insertions and removal of points, and Marot *et al.* [4] introduced a scalable parallelization scheme that uses Moore's curve for space partitioning. All these are multicore CPU algorithms working on point sets that do not handle the more complex cases of PLCs. For PLC, Chernikov and Chrisochoides [19] proposed an octree to partition the domain for triangulation to discover work that can be scheduled to run concurrently on multicore CPU. However, there are neither efficient scheduling algorithm nor experimental results known that can achieve good speedup. The latest known, with the use of multicore CPU, for a refinement problem (on point sets only) is in [4]. It experimented with Intel Core i7-6700HQ 4-core and AMD EPYC 64-core, but was only able to achieve a small single digit speedup, a result that is far from being effective on refinement in comparison to our approach of using (an inexpensive) GPU that achieves an order of magnitude speedup.

III. Exploring GPU for Refinement

The heart of refining a triangulation $\mathcal{T}$ is to add as many Steiner points as needed to eliminate bad tetrahedra. As bad tetrahedra possibly resulted from segments (or subsegments) and polygons (or subfaces), from the input, that are on their boundaries and are forced to appear in the output triangulation, Steiner points are also needed to split subsegments and subfaces into smaller ones. The center of the circumsphere of a bad tetrahedron, the center of the circumcircle of a subface, and the midpoint of a subsegment are points calculated as *splitting points* and some of them will be inserted as Steiner points of $\mathcal{T}$. Whenever a splitting point p becomes a Steiner point in $\mathcal{T}$, those tetrahedra whose circumspheres enclose p and interior points visible to p have to be eliminated and be replaced by tetrahedra incident to p.

It is obvious then that the use of GPU to do refinement is to design a GPU-friendly algorithm to compute splitting points and add them as Steiner points, as needed, concurrently by thousands of GPU threads. This is to be repeated round after round while maintaining $\mathcal{T}$, a constrained Delaunay triangulation, until either no more bad tetrahedra, in the best case, or some unsplittable ones, that are futile to continue processing, are left.

To be GPU-friendly, an algorithm launching concurrently with thousands of GPU threads at each step would want threads to have balanced workload and regularized work to maximize the utilization of GPU capacity. This results in a number of design considerations which are unique to GPU parallel computation and do not exist in a sequential CPU one. These considerations are discussed in the following subsections with each addressed by our algorithm in the corresponding subsection in Section IV.

A. Priorities of Splitting Points

It is natural to think of using one GPU thread to calculate a splitting point, locate it within some tetrahedron of $\mathcal{T}$, and then add it as a Steiner point. However, any two Steiner points inserted concurrently in the same round must be so-called *Delaunay independent*, i.e., they must not form an edge (which can be too short) in $\mathcal{T}$, so as to avoid non-termination of the algorithm. For a splitting point p, its *Delaunay region* [20] is defined as the union of tetrahedra in $\mathcal{T}$ whose circumspheres enclose p and whose interior points are visible to p. When two splitting points are such that the intersection of their Delaunay regions contain at most some vertices or edges of $\mathcal{T}$, they are indeed Delaunay independent. So, the goal is to design an algorithm to allow the insertion of many, if not all, splitting points with mutually disjoint Delaunay regions. Unavoidably, the algorithm needs to prioritize among all splitting points to retain a subset with mutually disjoint Delaunay regions for concurrent insertions.

B. Supporting Data Structures

For computations on triangulations, the standard tetrahedron-based data structure [21] supports stepping (walking) from one element, either vertex, edge, face, or tetrahedron, to any of its neighbor in constant time.[2] With it, a GPU thread can take linear time (to the number of tetrahedra in the Delaunay region) to identify the Delaunay region for a splitting point. However, Delaunay regions often come in different sizes and thus the handling of each region by one GPU thread would result in unbalanced workload among thousands of concurrent GPU threads. In this way, the task for a GPU thread to decide whether a Delaunay region overlaps some others would not be a balanced workload computation either. Moreover, this computation is needed for each splitting point, regardless of whether it eventually becomes a Steiner point, and thus on the whole undoubtedly taking away lots of computing power of the GPU. Most of these computations are verification in nature and do not contribute directly to refining a triangulation as they are not needed in any CPU algorithm. Therefore, such "inessential" computations in GPU must be done efficiently to waste little computing time to pay for identifying a large subset of splitting points with mutually disjoint Delaunay regions for concurrent insertions. To this end, using one GPU thread, supported with only the standard tetrahedron-based data structure (as in the CPU algorithm), to compute a Delaunay region is not a wise approach.

C. Cavity Growing

One idea to avoid wasting the computation of Delaunay regions is to piggyback this to the actual insertion of a splitting point as a Steiner point. That is, a splitting point p is pretended to be a Steiner point of $\mathcal{T}$ and flipping is carried out to restore the Delaunay property of $\mathcal{T}$ and in turn also identify the Delaunay region of p. When flips of different splitting points collide (i.e., their Delaunay regions are found to overlap), some flips for one splitting point will be undone. Such a strategy was employed successfully for the 2D problem [9]. It is, however, unclear whether this can work for 3D problems since flipping (to undo some earlier flips) is not known to be able to reach all possible triangulations [23]. As a consequence, an algorithm with mainly (parallel) flipping can be stuck at a state where it does not know how to restore to some old state with more flipping. Hence, the computation of Delaunay regions has to be decoupled from the insertion of splitting points with GPU threads. In order to compute a Delaunay region, the next alternative is to systematically grow the so-called *cavity*. Initially, the cavity of a splitting point p is the collection of tetrahedra incident to or containing p. The cavity is then grown by progressively adding tetrahedra, which have their circumspheres enclosing p, incident to the boundary of the current cavity. In other words, the cavity is a partial Delaunay region growing towards a Delaunay region. Whichever the approach may be, an algorithm has to employ concurrent GPU threads with regularized work to grow cavities.

D. Cavity Shrinking

Because we work with the constrained Delaunay triangulation, a Delaunay region of a splitting point p only includes tetrahedra whose interiors are visible to p besides having p inside their circumspheres. As such, the growing of the cavity of p should stop once it hits some subface that occludes the visibility. Such stopping can shield away subsegments and subfaces that are invisible but may prohibit the insertion of

[2] We adapt the usual practice used in [22] to have an infinite vertex to connect to all boundary faces of the triangulation to form "ghost" tetrahedra, and to all boundaries of input polygons of F in $\mathcal{G}$ to form "ghost" subfaces.

p before their splittings. Hence, without knowing what have been occluded, a decision to proceed to insert p may be premature and can result in the need to remove p in subsequent processing (which can be costly under a parallel setting; see [5]). Considering this, we need to weigh the advantage of saving some computation by growing the cavity without considering the visibility against the disadvantage of shrinking to amend the cavity to its Delaunay region.

E. Termination

All in all, any refinement algorithm must be mindful to still terminate while adding many Steiner points concurrently. In our algorithm, splitting points are computed and located in tetrahedra, then they are filtered out in different stages to leave behind only those that are Delaunay independent for insertions. The filtering starts immediately after the splitting points are located in tetrahedra where each tetrahedron can only house one splitting point. Then, the growing of cavities is meant for splitting points to gradually obtain their complete Delaunay regions; those which cannot complete are filtered out. Before shrinking the cavity of the splitting point of an element e, this cavity is aborted if there are other subsegments or subfaces which are supposed to be split before e because their dimensions are lower than that of e. A final check is used to ensure that the splitting points of completed Delaunay regions are indeed Delaunay independent and that these splitting points can be inserted as Steiner points to create new tetrahedra to complete this round of concurrent point insertions.

IV. Our Proposed Algorithm

Our proposed GPU algorithm is depicted in Algorithm 1 as `gQM3D`. For an input PLC $\mathcal{G}$, we can assume its CDT exists or we use the approach in [24] to split its edges to guarantee so. We thus discuss our algorithm with an input constant B and a CDT $\mathcal{T}$ of $\mathcal{G}$ that has bad tetrahedra due for refinement. A subsegment or subface e is so-called *encroached* when there exists a point q, which is a vertex of $\mathcal{T}$ or a splitting point, inside the diametric sphere of e. In this case, q is called an *encroaching point* that *encroaches upon* e.

The algorithm `gQM3D` starts by recording encroached subsegments (Line 1 to 3), encroached subfaces (Line 4 to 6) and bad tetrahedra (Line 7 to 9) in the input CDT for refinement. Next, it refines encroached subsegments (Line 10, 25 and 32), encroached subfaces (Line 11 and 33) and bad tetrahedra (Line 12) in this order iteratively until `SplitBadTets` terminates with no more bad tetrahedra or only bad tetrahedra that are unsplittable. In every iteration of **repeat-until** in these routines, the elements, which are subsegments, subfaces and bad tetrahedra, to be split or eliminated are collected into the list M using stream compaction (Line 16, 22 and 29) and then passed to the pipeline of `InsertPoints` (Line 18, 24 and 31), a concurrent point insertion routine (see Section IV-A).

As designed, `gQM3D` gives higher priority to the splitting points of subsegments (lowest dimension) followed by those of subfaces and finally those of bad tetrahedra (highest dimension). This is natural as lower dimension problems must be solved before higher dimension ones. On another matter, our experiments show that `gQM3D` does not have any particular advantage over the CPU approach for splitting encroached subsegments and subfaces at Line 10 and 11. This is because such splittings take many rounds of point insertions but each does not have heavy workload to fill GPU capacity. This low utilization of GPU capacity is also observed for Line 32 and 33 in `SplitBadTets` due to the fact that the number of encroached subsegments and subfaces are generally small after Line 10 and 11. As such, a CPU-GPU hybrid variant called `gQM3D`$^+$, shown in Algorithm 2, is developed from `gQM3D` by making two adjustments: (1) it has Line 1 and 2 to split encroached subsegments and subfaces by `TetGen`

Algorithm 1: `gQM3D`

Input: CDT $\mathcal{T}$ of PLC $\mathcal{G}$; constant B
Output: Quality Mesh $\mathcal{T}$, which is also a CDT

`// Recording elements for refinement`
1 **for** *each subsegment* $s \in \mathcal{T}$ ***in parallel*** **do**
2   **if** *the diametric sphere of* s *encloses any vertex of* $\mathcal{T}$ **then**
3   Record s as encroached in $\mathcal{T}$
4 **for** *each subface* $f \in \mathcal{T}$ ***in parallel*** **do**
5   **if** *the diametric sphere of* f *encloses any vertex of* $\mathcal{T}$ **then**
6   Record f as encroached in $\mathcal{T}$
7 **for** *each tetrahedron* $t \in \mathcal{T}$ ***in parallel*** **do**
8   **if** *the radius-edge ratio of* t *is larger than* B **then**
9   Record t as a bad tetrahedron in $\mathcal{T}$

`// Refinement steps`
10 `SplitEncSubsegments`$(\mathcal{T}, B)$
11 `SplitEncSubfaces`$(\mathcal{T}, B)$
12 `SplitBadTets`$(\mathcal{T}, B)$
13 **End**

`// Routine definitions`
14 **Procedure** `SplitEncSubsegments`$(\mathcal{T}, B)$
15   **repeat**
16   Collect all encroached subsegments into list M in parallel
17   **if** $M \neq \emptyset$ **then**
18   `InsertPoints`$(\mathcal{T}, M, B)$
19   **until** $M = \emptyset$
20 **Procedure** `SplitEncSubfaces`$(\mathcal{T}, B)$
21   **repeat**
22   Collect all encroached subfaces into list M in parallel
23   **if** $M \neq \emptyset$ **then**
24   `InsertPoints`$(\mathcal{T}, M, B)$
25   `SplitEncSubsegments`$(\mathcal{T}, B)$
26   **until** $M = \emptyset$
27 **Procedure** `SplitBadTets`$(\mathcal{T}, B)$
28   **repeat**
29   Collect all bad tetrahedra into list M in parallel
30   **if** $M \neq \emptyset$ **then**
31   `InsertPoints`$(\mathcal{T}, M, B)$
32   `SplitEncSubsegments`$(\mathcal{T}, B)$
33   `SplitEncSubfaces`$(\mathcal{T}, B)$
34   **until** $M = \emptyset$

Algorithm 2: gQM3D$^+$

```
   Input: CDT 𝒯 of PLC 𝒢; constant B
   Output: Quality Mesh 𝒯, which is also a CDT
   // Refinement steps on the CPU
1  SplitEncSubsegments_CPU(𝒯, B)
2  SplitEncSubfaces_CPU(𝒯, B)
3  Copy 𝒯 from CPU to GPU
   // Refinement steps on the GPU
4  Line 1 to 9 as in Algorithm 1
5  SplitBadElements(𝒯, B)
6  End
   // Routine definitions
7  Procedure SplitBadElements(𝒯, B)
8  |  repeat
9  |  |  Collect all encroached subsegments, subfaces and
   |  |    bad tetrahedra into list M in parallel
10 |  |  if M ≠ ∅ then
11 |  |  |_ InsertPoints(𝒯, M, B)
12 |_ until M = ∅
```

in CPU, which correspond to Line 10 and 11 of gQM3D, respectively; and (2) it replaces SplitBadTets (Line 12) of gQM3D by SplitBadElements (Line 5), which processes all elements of different types in one single routine, and still respects the priority of processing elements from lower to higher dimensions. In this way, the leftover capacity of GPU during the splitting of subsegments and subfaces can be utilized to eliminate bad tetrahedra to gain good speedup. Note that if the first adjustment is not employed, gQM3D$^+$ can remain as a pure GPU algorithm, like gQM3D.

A. Concurrent Point Insertions Pipeline

Both gQM3D and gQM3D$^+$ rely on InsertPoints to achieve high parallelism. It takes a set of elements, each an encroached subsegment, encroached subface or bad tetrahedron as input to decide a subset of these elements to be split concurrently while ensuring termination of the algorithm. For gQM3D, it processes a set of homogeneous elements of either encroached subsegments, encroached subfaces or bad tetrahedra, individually and not a mixture of them. On the other hand, for gQM3D$^+$, all the different types of elements can be processed at the same time while still respecting higher priorities for lower than higher dimension elements.

There are four distinct stages in InsertPoints, each is one or more kernel programs running in GPU: (a) splitting points calculation and location, (b) cavity growing for splitting points, (c) cavity shrinking for splitting points, and (d) cavity remeshing (or re-triangulation) for inserting splitting points.

Stage (a) calculates splitting points of input elements using a kernel program with one GPU thread handling one input element to output one splitting point (which is the midpoint of an encroached subsegment, or circumcenter of an encroached subface or bad tetrahedron). Another kernel program with one GPU thread handling one element will then be used to step, starting from the element, from tetrahedron to tetrahedron in $\mathcal{T}$, to locate the one containing its splitting point. Each tetrahedron is allowed to contain at most one splitting point. As such, when two splitting points are found to be in the same tetrahedron, only the splitting point with the higher priority is kept for subsequent computation while the other is filtered away. As mentioned, lower dimension elements have higher priorities than higher dimension elements. Between two elements of the same dimension, it is found through our experiments that the element with a larger measure (length for subsegment, area for subface, and volume for bad tetrahedra) should be given a higher priority to achieve a better speedup. This can be understood as breaking up larger elements early can create more work to better utilize GPU capacity.

Stages (b) to (c) are designed to achieve balanced workload by GPU threads and together with Stage (d) are elaborated in the next three subsections. In a nutshell, they are stages that employ parallel prefix and stream compaction on list structures to further filter out splitting points till the remaining splitting points are indeed mutually Delaunay independent. All these splitting points can then be inserted to refine the triangulation in Stage (d) while ensuring that the algorithm terminates. Each tetrahedron in the triangulation can belong to at most one cavity of a splitting point. When two splitting points compete to own the same tetrahedron due to their overlapping Delaunay region, we use the same priority as mentioned in the previous paragraph to decide which splitting point can continue the processing.

B. Supporting Cavity Computation with Tuples

Besides the mentioned standard tetrahedron-based data structure to represent the triangulation, we use *tuples* stored in lists (arrays) in the GPU global memory to support computations by thousands of concurrent GPU threads. For a tetrahedron t with its one face f, we write it as a tuple $\langle t, f\rangle$. Then, the tetrahedron t' sharing the face f with t, which can be obtained in constant time from the standard tetrahedron-based data structure, is written as $\langle t', f\rangle$. For an element e with an associated splitting point p, we write $\langle e, \langle t, f\rangle\rangle$ to mean that face f of tetrahedron t is relevant in some way to the computation of the cavity of p. In one instance of the growing of a cavity, such a tuple in the list L means t is a tetrahedron in the cavity of p and any tetrahedron sharing face f with t will be explored as part of the Delaunay region of p (see Figure 3 for an example). In another instance of shrinking a cavity, such a tuple in the list $\overline{L}$ means t is a tetrahedron with face f bounding the Delaunay region of p.

Let us take a peep into the growing of a cavity using the list L to further understand the role of tuples in realizing balanced workload for concurrent GPU threads in a highly regularized work manner. For each tuple, one GPU thread is assigned to check how many tuples, zero to three, it will contribute to the list in each iteration. Since the maximum number here is three, after a parallel prefix calculation, any newly generated tuple can be added in constant time to L at some designated index. After that, as not all reserved indices are used, L can be compacted to obtain consecutive indices containing newly generated tuples for the next iteration of computation.

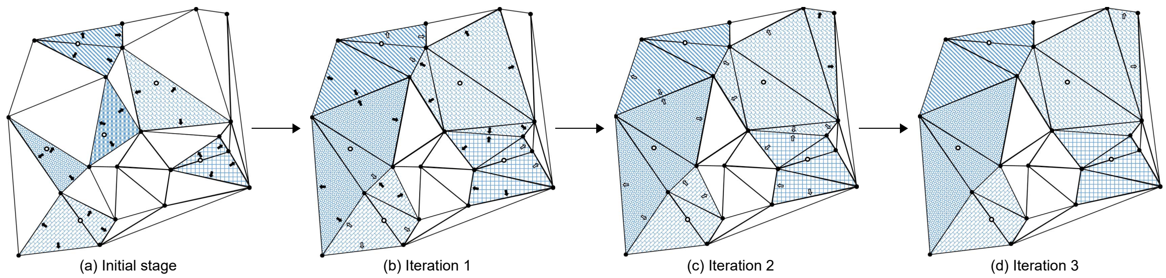

Fig. 2. An illustration of the growing of cavities in 2D. (a) Initially, there are 6 splitting points drawn as hollow circles with their initial cavities shown in different grid patterns. A black arrow pointing to an edge h of a triangle f in the cavity of a splitting point p of element e is a tuple $\langle e, \langle f, h\rangle\rangle$ in L. For each tuple, a GPU thread will perform the `incircle` test of p inside the circumcircle of f' where f' shares h with f, and attempt to grow the cavity of p by including the tuple $\langle e, \langle f', h'\rangle\rangle$ and $\langle e, \langle f', h''\rangle\rangle$ to L where h', h'' are the other two edges of f'. (b) In iteration 1, the growing of the cavity for one splitting point near the center was unsuccessful due to its presumably lower priority than those of other competing cavities, and this splitting point is removed from the picture. The growing of the others were successful as shown with black arrows as new tuples added to L. Note that each white arrow indicates the failure of an `incircle` test for a tuple, and this tuple is added into $\overline{L}$. (c) All cavities of splitting points, except for the top-right one, stopped growing. (d) As there are no more successful `incircle` test to add new tuples into L, the cavity growing is complete.

Also, tuples that are no longer needed (in the current or past iterations) can be filtered out by compaction to conserve storage and to prevent themselves from being involved in irrelevant computations subsequently. On the whole, L is an effective and efficient linear structure to contain results obtained in each iteration. We can then deduce from L a set of tetrahedra in the Delaunay region of each splitting point.

C. Cavity Growing with Multiple Threads

Instead of the approach of growing with respect to visibility, we design a grow-and-shrink scheme to compute cavities of splitting points using GPU. This decision is justified by our experiments which showed that on the whole, our approach reduces the computations required since shrinking cavities do not require as much computations as growing them. More importantly, our approach avoids the insertion of inappropriate splitting points that will need to be undone painfully in the parallel computation setting. This subsection discusses the growing portion while the shrinking portion will be discussed in the next subsection. See Figure 2 for an illustration of the growing of cavities in 2D.

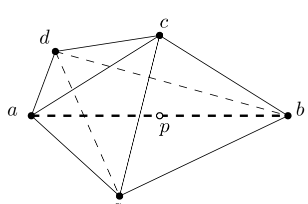

Fig. 3. An example where splitting point p is on subsegment ab. It intersects two subfaces abc and abg, and three tetrahedra $abcd$, $abcg$ and $abdg$. For splitting point p, the list L used in growing cavities is initialized with $\langle ab, \langle abcd, acd\rangle\rangle$, $\langle ab, \langle abcd, bcd\rangle\rangle$, $\langle ab, \langle abcg, acg\rangle\rangle$, $\langle ab, \langle abcg, bcg\rangle\rangle$, $\langle ab, \langle abdg, adg\rangle\rangle$, and $\langle ab, \langle abdg, bdg\rangle\rangle$. For splitting point p, the list used in growing its subface cavity is initialized with $\langle ab, \langle abc, ac\rangle\rangle$, $\langle ab, \langle abc, bc\rangle\rangle$, $\langle ab, \langle abg, ag\rangle\rangle$, and $\langle ab, \langle abg, bg\rangle\rangle$. Suppose now that abd is also a subface, then $\langle ab, \langle abd, ad\rangle\rangle$ and $\langle ab, \langle abd, bd\rangle\rangle$ are also included to initialize the list to grow the subface cavity of p.

Let e be an element, either a bad tetrahedron, a subface, or a subsegment. The algorithm either grows the cavity of its splitting point p until the cavity becomes the Delaunay region of p or is terminated by an overlapping cavity of another element of a higher priority. The entire process is carried out with GPU threads operating on the list L, where each entry is a tuple. Initially, one GPU thread is used to handle one splitting point p of an element e to collect all tetrahedra intersecting p, denoted as $\cap(p)$, into L. That is, all tuples in $\{\langle e, \langle t, f\rangle\rangle | f \text{ is a triangle of } t \in \cap(p) \text{ and } f \cap p = \emptyset\}$ are added into L; refer to Figure 3 for an illustration. However, we need to ensure that each tetrahedron can only be included in at most one tuple, i.e., in one cavity. To do this, the standard two-step process is employed: an element e is to first mark a tetrahedron t, using the atomic operation to set t to the priority of e, to be a part of the cavity of the splitting point of e. After all markings by elements are synchronized, those who successfully marked their tetrahedra can then add the corresponding tuples into L. On the other hand, if an element e fails to mark some tetrahedron, it means that it has a low priority and its splitting point p has an overlapping Delaunay region with those of elements of higher priorities. This causes the cavity of p to stop growing, and p is filtered out for the current round of point insertions.

Next, we grow cavities further based on those initial tuples in L as follows:

(1) Let one GPU thread handle one tuple $\langle e, \langle t, f\rangle\rangle$ of splitting point p to find the neighbor of $\langle t, f\rangle$ termed as $\langle t', f\rangle$. If t' passes the `insphere` test, i.e., its circumsphere encloses the splitting point p of e, then e attempts to mark t' to be in the cavity of p (in the two-step process as mentioned above). If e fails to mark t', the growing of the cavity of p is aborted and all tuples related to e will no longer be involved in subsequent processing. At this step, it is also possible that e successfully marks t' that was already in the cavity of a splitting point q of another element, then the cavity of q is to be aborted.

(2) Let one GPU thread handle one tuple $\langle e, \langle t, f\rangle\rangle$ of

splitting point p to find the neighbor of $\langle t, f\rangle$ termed as $\langle t', f\rangle$. If t' passes the `insphere` test, then we add all tuples in $\{\langle e, \langle t', f'\rangle\rangle | f' \neq f$ is a triangle of $t'\}$ to L; otherwise, we add $\langle e, \langle t', f\rangle\rangle$ to $\overline{L}$, which is a list to keep track of all tetrahedra which failed the `insphere` test and are to be used subsequently in the shrinking of cavities.

(3) If new tuples were added to L in Step 2, go to Step 1 and repeat the process for the new tuples; otherwise stop.

When the above terminates, each element with tuples that always succeeded in marking tetrahedra during the process has identified the (more than) complete Delaunay region of its splitting point. Moreover, all such Delaunay regions of splitting points are disjoint.

The above works for cavities that are formed by collections of tetrahedra. As subfaces are constraints from the input that we need to split into smaller ones in the output, we also need to identify the so-called *subface cavities*. The process of growing with triangles in a subface cavity here has the same structure as that of growing with tetrahedra in a cavity with the following adjustments: (1) the `incircle` test, which decides whether a point is inside a circumcircle of a triangle, is used instead of the `insphere` test; and (2) growing with triangles is to respect the visibility and thus does not cross any subsegment, while growing with tetrahedra can cross subfaces.

Though the above has identified splitting points with disjoint Delaunay regions, not all splitting points can be inserted into $\mathcal{T}$ as yet. We do not insert splitting points of bad tetrahedra that encroach upon existing subfaces or subsegments, and do not insert those of subfaces that encroach upon existing subsegments. Such splitting points have to wait until later rounds after those encroached subfaces and encroached subsegments have been split. This is to respect the priority of splitting elements of lower dimensions before those of higher dimensions. The growing of a cavity without concerning occlusions due to subfaces, in our algorithm, allows us to easily identify those splitting points that are not good for insertion as follows: we assign one GPU thread to handle one tuple, $\langle e, \langle t, f\rangle\rangle$, in L where p is the splitting point of e. If e is a bad tetrahedron and f is a subface, we check whether f is encroached by p; if e is a subface or a bad tetrahedron and f is bounded by some subsegments, we check whether any such subsegment is encroached by p. If so, p is to be filtered out in the current round of point insertions; see Figure 4. In the above process, if p is not filtered out and f is a subface, we record $\langle e, f\rangle$ in a list called L_s for use in the shrinking of cavities.

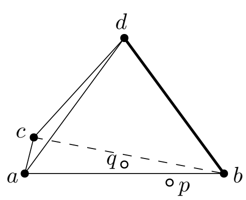

Fig. 4. An example where p is the splitting point of some bad tetrahedron with its cavity grown to include subface abc and subsegment bd. As p encroaches upon abc, it cannot be inserted before the insertion of the center q of the circumcircle of abc. In this example, q in turn encroaches upon bd and thus cannot be inserted until bd has been split into two subsegments. In another setting, it can happen that p encroaches upon bd but not necessarily abc. Because visibility was not taken into consideration in the growing of the cavity of p, all these encroachments are discovered in time to avoid any unnecessary attempts to insert p or q before splitting bd.

D. Cavity Shrinking with Multiple Threads

Since the growing of cavities does not respect the visibility, we need to fix it by shrinking cavities, using L_s. For each tuple $\langle e, f\rangle$ in L_s where p is the splitting point of e, one GPU thread is used to check whether f is an interior subface of the cavity of p. It is so when the two incident tetrahedra of f are marked with the priority of e. In this case, we mark the tetrahedron t with a vertex on the opposite side to p with respect to f as no longer a part of the Delaunay region of p because it is invisible to p. With t, we add four tuples in $\{\langle e, \langle t, f'\rangle\rangle | f'$ is a face of $t\}$ to $\overline{L}$ (which already contains, from the cavity growing stage, those tetrahedra failing the `insphere` test) and start the shrinking process as follows:

(1) Let one GPU thread handle one tuple $\langle e, \langle t, f\rangle\rangle$ in $\overline{L}$ and find the neighbor of $\langle t, f\rangle$ termed as $\langle t', f\rangle$. Let v be the vertex of t' not in f. If v and p are on different sides of the plane passing through f, we mark t' as no longer in the Delaunay region of p, and add all tuples in $\{\langle e, \langle t', f'\rangle\rangle | f' \neq f$ is a triangle of $t'\}$ to $\overline{L}$; see $\langle acgi, acg\rangle$ in Figure 5. Otherwise, we add $\langle e, \langle t', f\rangle\rangle$ to L_r, which is a list to keep track of tuples for use in remeshing; see $\langle abcd, abc\rangle$ in Figure 5.

(2) If new tuples were added to $\overline{L}$ in Step 1, go to Step 1 to repeat the process for the new tuples; otherwise stop.

Once the above process terminates, all tetrahedra that are no longer in any Delaunay regions would have been added to $\overline{L}$. The list L can also be updated through $\overline{L}$ to keep only tuples (of tetrahedra) of Delaunay regions. Till here, there is still one more filtering that needs to be done to L to keep only splitting points that are indeed mutually Delaunay independent. For any

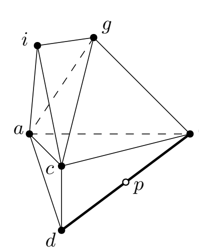

Fig. 5. An example where p is the splitting point of subsegment bd and abc is a subface in the cavity of p. Initially, both $\langle bd, \langle abcg, acg\rangle\rangle$ and $\langle bd, \langle abcg, abc\rangle\rangle$ (and two other tuples $\langle bd, \langle abcg, bcg\rangle\rangle$ and $\langle bd, \langle abcg, abg\rangle\rangle$) are added into $\overline{L}$. For the former, its neighbor is $\langle acgi, acg\rangle$ with i and p on different sides of acg. Thus, $acgi$ is marked as no longer in the Delaunay region of p, and three new tuples $\langle bd, \langle acgi, aci\rangle\rangle$, $\langle bd, \langle acgi, cgi\rangle\rangle$, and $\langle bd, \langle acgi, agi\rangle\rangle$ are added into $\overline{L}$ for further exploration. As for the latter, its neighbor $\langle abcd, abc\rangle$ has vertex d and p on the same side of abc, and this neighbor thus remains in the Delaunay region of p and is added to L_r for use in remeshing.

two splitting points p and q, they are Delaunay independent if the intersection of their Delaunay regions is empty or contains at most some vertices, edges or subfaces of $\mathcal{T}$. Now, for the Delaunay regions sharing a triangle f, splitting points p and q may not be Delaunay independent and we need to filter out one of them; see Figure 6. To check this, we use one GPU thread to check each tuple $\langle e, \langle t, f\rangle\rangle$ in L: if f is not a subface and is incident to two tetrahedra (one being t) belonging to two different Delaunay regions of two splitting points, p (of e) and q (of another element), then check if q is in the circumsphere of the tetrahedron formed by p and f. If so, the one with lower priority, either p or q, is filtered out. With this, all splitting points that remain are indeed Delaunay independent and they are ready to be inserted into $\mathcal{T}$.

For the purpose of remeshing the Delaunay regions, we next need to derive the boundary tetrahedra of the Delaunay regions from L_r. A tuple $\langle e, \langle t, f\rangle\rangle$ was added into L_r because it is uncertain whether t is inside the cavity of the splitting point of e and subsequent processing may mark t to be outside the cavity. We thus assign one GPU thread to handle one tuple $\langle e, \langle t, f\rangle\rangle$ in L_r and remove it from L_r if t is no longer marked by the priority of e. In doing so, we are left with tetrahedra that are truly inside some cavities. We can then reuse $\overline{L}$ by first setting it to empty, and then using each tuple $\langle e, \langle t, f\rangle\rangle$ in L_r to identify its neighbor t', which shares f on the boundary of a Delaunay region, to store $\langle e, \langle t', f\rangle\rangle$ into $\overline{L}$ for remeshing Delaunay regions.

Given all boundary tetrahedra in $\overline{L}$, we assign one GPU thread to handle one tuple $\langle e, \langle t, f\rangle\rangle$ in $\overline{L}$ to create a new tetrahedron formed by f and the splitting point p of e. Next, we update the neighborhood information in two parts. First, each new tetrahedron has one neighbor, which is available in $\overline{L}$ and outside the cavity, that can be updated straightforwardly. Second, two new tetrahedra adjacent to each other inside the same cavity need to be updated as neighbors. This is achieved for each such tetrahedron t by stepping from tetrahedron to tetrahedron outside the cavity and around an edge of t until its neighbor inside the cavity is reached.

Likewise, from $\langle e, \langle f, h\rangle\rangle$ in the list that records subface cavity, we can create a new subface formed by edge h and the splitting point p of e. In addition, if a splitting point p is on a subsegment ab, we create two new subsegments pa and pb. The updating of the neighborhood information of new subfaces and new subsegments are done straightforwardly.

E. Ensuring Termination of Concurrent Insertions

The algorithm terminates when there are no bad tetrahedra or some *unsplittable* bad tetrahedra left. The latter are bad tetrahedra whose removal would result in the introduction of other bad tetrahedra into $\mathcal{T}$, and thus it is futile to continue processing them. The unsplittable concept was introduced to handle small input angles formed by segments and polygons. It relies on the so-called *insertion radius* [25]. For a vertex p in the triangulation $\mathcal{T}$, its insertion radius is the length of the shortest edge connected to p when p is inserted into $\mathcal{T}$. In practice, the insertion radius is usually *relaxed* (or enlarged) to prevent never-ending point insertions; see Figure 7. For our purpose, we set an element e with a splitting point p to be unsplittable if all elements encroached by p are unsplittable. This is understandable as there is no way to insert p if those to be split or eliminated before e are already unsplittable.

To sum up, our algorithm inserts only a finite number of Steiner points into the triangulation $\mathcal{T}$ as it maintains a lower bound on the lengths of the edges within a finite space, and it thus terminates in finite time. In the following explanation, we have adapted the argument in [2] to guarantee the existence of this lower bound. The *local feature size* for a point p, denoted as $lfs(p)$, in the PLC $\mathcal{G}$ is the radius of the smallest sphere centered at p that intersects two non-incident elements in $\mathcal{G}$. To facilitate the argument, the insertion radius of a splitting point filtered out due to encroachment (such as p and q in Figure 4) is defined in the same way as if it were inserted into $\mathcal{T}$. We can then form a directed graph by connecting a Steiner point to another point that defined its insertion radius. The latter point is either an input point of $\mathcal{G}$, another Steiner point inserted earlier or a splitting point filtered out due to encroachment. The graph shows that the insertion radius of one Steiner point can be traced and lower bounded by following the directed edges, all the way until the $lfs(p)$ of a point p of $\mathcal{G}$. This is true when $B > 2$ and $\mathcal{G}$ has no two edges or polygons forming an acute angle [2]. For the latter, those elements around small angles are treated in the algorithm as unsplittable and unable to cause non-termination. They can thus be omitted in this

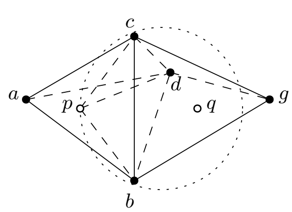

Fig. 6. p and q are splitting points with $abcd$ and $bcdg$, respectively, in their Delaunay regions sharing bcd that is not a subface. If both p and q are inserted concurrently, then the circumsphere of the new tetrahedron $bcdp$ encloses q (and that of $bcdq$ encloses p). So, bcd is not Delaunay and does not appear in the new $\mathcal{T}$, while p and q are Delaunay dependent and appears as pq in the new $\mathcal{T}$.

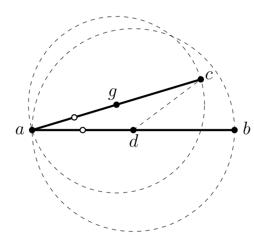

Fig. 7. Subsegments ac and ab form a small input angle, $\angle cab$. Thus, vertex c encroaches upon ab, which is split at d. Vertex d encroaches upon ac, which is split at g. The insertion radius of d is $|cd|$ and that of g is relaxed to $|cd|$ as well. Both ag and ad are set as unsplittable because splitting them would create edges shorter than $|cd|$.

discussion. Hence, the smallest $lfs(p)$ bounds all the lengths of edges in $\mathcal{T}$.

V. Experimental Results

All experiments were conducted on a PC with an Intel i7-7700k 4.2GHz CPU, 32GB of DDR4 RAM and a GTX1080 Ti graphics card with 11GB of video memory.

A. Software Used for Comparison

`TetGen` [3] is the main CPU software used as benchmark for our work. Since `CGAL` [16] is a popular software in this area, though its output often does not conform to its input PLC, we incorporated it in our experiments with edge_size = 5.0, facet_distance = 1.0 and cell_radius_edge_ratio = B. As for `TetWild` [17] that mainly focuses on robustness, it runs rather slowly and is thus excluded from our study.

We implemented `gQM3D` and `gQM3D`$^+$ using the CUDA programming model of NVIDIA [26]. All computations in GPU are done with the double precision. The exact arithmetic and robust geometric predicates of Shewchuk [27] are adapted from CPU to work in GPU. Simulation of Simplicity by Edelsbrunner and Mücke [28] is used to deal with degenerate cases.

In our implementation, we chose to stop the growing of a cavity when it ran beyond a large number of iterations, such as in the case of a degenerate tetrahedron. We set such a tetrahedron to unsplittable when encountered. This, however, did not result in any significant increase in the number of bad tetrahedra in the outputs of our experiments. In another aspect, we noticed that a cavity of p that caused another of say q to stop growing, may itself be forbidden to be grown by other cavities. The question is then whether it is worthwhile to revive the growing of the cavity of q since its needed tetrahedra are now made available through p. With regards to this, we have attempted some approaches in our implementation but have yet to find any good one which improves performance.

All software were compiled with all optimization flags turned on. The input to all software is a PLC with a constant B. We used `TetGen` to generate the initial CDT (that has bad tetrahedra) to be refined by `gQM3D` and `gQM3D`$^+$. In measuring computing time, we included the time of computing the CDT of the input PLC in all software. We have done experiments on both synthetic and real-world datasets as reported in the following two subsections.

B. Synthetic Dataset

To better understand the behavior of the various software and to stress test them, we generated PLCs with points in the following distributions: uniform, Gaussian, ball (where points lie randomly in a ball) and sphere (where points lie randomly within the thin shell formed by two concentric spheres with different radii). Also, we randomly generated polygons that are rectangles to add into our PLCs. While edges of rectangles may form small input angles among themselves, we ensured that there were no intersections among them, except at their endpoints.

The number of input points in each PLC is between 10K to 30K, while the ratio of the number of rectangles to the number of points, denoted as γ, ranges from 0.05 to 0.25. These parameters were chosen to stress test `gQM3D` and `gQM3D`$^+$ by exhausting the available GPU memory, which supports output sizes of over tens of millions of points and tetrahedra. Although the termination of the various software requires $B > 2$ and input angles no less than $90°$, this is less onerous in practice. We thus tried a spread of B, around 2, and let `gQM3D` and `gQM3D`$^+$ adapt the same approach as `TetGen` to handle elements in the vicinity of small input angles. Consequently, the output triangulations can contain some bad tetrahedra that are unsplittable due to small input angles.

Running Time

The running time of `gQM3D` and `gQM3D`$^+$ includes the time for computation, as well as, the time needed to transfer data between CPU and GPU. For each input, we repeated many runs and recorded its average timing and triangulation quality for reporting here. Table I is obtained with 25K input points under the ball distribution; findings with the other distributions and different input point sizes are the same and their details are thus omitted. We observe that `TetGen` at time needed close to an hour to complete its computation, while `gQM3D` and `gQM3D`$^+$ can complete within a few minutes.

The trend of the speedup achieved by using `gQM3D` and `gQM3D`$^+$ over `TetGen` for all the distributions are shown in Figure 8 where some curves for the different B are omitted for clarity. The speedup increases with γ but decreases with B for all distributions. This is within expectation as a larger γ with a smaller B means more subfaces (thus more bad tetrahedra) are available for concurrent processing with thousands of GPU threads. As a result, `gQM3D` and `gQM3D`$^+$ can achieve speedup of an order of magnitude. Across the four distributions, for each γ, we note that `gQM3D` and `gQM3D`$^+$ have consistently achieved a higher speedup with the ball distribution, while having comparable performance on the other three. As for the comparison to `CGAL`, both `gQM3D` and `gQM3D`$^+$ remain many times faster and with much fewer numbers of bad tetrahedra; see Table I.

Timing Breakdown

Figure 9 shows that the time spent for Line 10 and 11 in `gQM3D` using GPU (see the bottom 2 portions in each bar of Figure 9(a)) is much longer than that of the corresponding work done by Line 1 and 2 in `gQM3D`$^+$ (see the bottom 2 portions in each bar of Figure 9(b) with the bottom-most portion hardly visible). This also implies that the speedup over `TetGen` in our implementation comes from `SplitBadTets` (Line 12) in `gQM3D` and `SplitBadElements` (Line 5) in `gQM3D`$^+$. This is indeed the case as shown in Figure 10, for the sphere distribution, and the results for the other distributions are similar.

Furthermore, we observe that `SplitBadElements` is faster than `SplitBadTets`. Figure 11 is plotted to understand the number of Steiner points inserted concurrently during

γ	0.05				0.10				0.15				0.20				0.25			
Software / B	CGAL	TetGen	gQM3D	gQM3D$^+$	CGAL	TetGen	gQM3D	gQM3D$^+$	CGAL	TetGen	gQM3D	gQM3D$^+$	CGAL	TetGen	gQM3D	gQM3D$^+$	CGAL	TetGen	gQM3D	gQM3D$^+$
1.4																				
Time (min)	2.8	2.5	1.3	0.5	6.9	6.6	2.2	0.9	11.1	20.4	3.1	1.7	15.7	28.6	3.9	1.9	21.3	53.4	4.5	2.5
Points (M)	0.78	0.95	0.93	0.96	1.46	1.52	1.49	1.54	2.09	2.63	2.59	2.67	2.62	3.11	3.06	3.16	3.24	4.24	4.18	4.29
Tets (M)	4.99	5.98	5.85	6.07	9.29	9.58	9.40	9.74	13.29	16.68	16.37	16.89	16.65	19.67	19.35	20.01	20.57	26.89	26.44	27.24
Bad Tets	$> 1M$	401	308	391	$> 2M$	1461	1416	1485	$> 2M$	2160	2059	2230	$> 3M$	2885	2939	2871	$> 4M$	3677	3395	3680
1.6																				
Time (min)	2.7	1.6	1.1	0.4	6.5	4.1	1.9	0.8	10.5	12.8	3.4	1.4	15.0	18.3	3.4	1.7	20.8	34.3	4.1	2.3
Points (M)	0.66	0.68	0.69	0.69	1.22	1.12	1.13	1.13	1.74	2.03	2.06	2.05	2.19	2.39	2.44	2.42	2.70	3.33	3.39	3.37
Tets (M)	4.19	4.27	4.33	4.33	7.76	7.00	7.10	7.09	11.10	12.73	12.91	12.90	13.91	15.06	15.29	15.26	17.17	20.94	21.28	21.24
Bad Tets	$> 0.8M$	303	252	313	$> 1M$	1279	1152	1212	$> 2M$	1877	1725	1870	$> 2M$	2520	2355	2472	$> 3M$	3235	2924	3261
1.8																				
Time (min)	2.6	1.1	1.1	0.4	6.3	2.9	1.7	0.7	10.2	9.0	2.5	1.3	14.2	12.8	3.3	1.6	19.3	24.1	4.6	2.0
Points (M)	0.59	0.56	0.57	0.57	1.09	0.92	0.95	0.94	1.55	1.73	1.79	1.75	1.95	2.05	2.12	2.07	2.40	2.88	2.97	2.93
Tets (M)	3.76	3.46	3.57	3.53	6.90	5.74	5.93	5.83	9.87	10.76	11.10	10.92	12.38	12.75	13.16	12.92	15.29	17.94	18.51	18.27
Bad Tets	$> 0.7M$	251	229	250	$> 1M$	1083	1467	1122	$> 1M$	1599	1473	1585	$> 2M$	1998	2004	1978	$> 2M$	2696	2484	2708
2.0																				
Time (min)	2.4	0.8	1.0	0.3	5.9	2.2	1.8	0.6	9.4	6.9	2.6	1.2	13.3	9.7	3.1	1.5	18.3	18.5	3.6	1.9
Points (M)	0.55	0.49	0.51	0.50	1.00	0.82	0.85	0.83	1.43	1.57	1.62	1.60	1.80	1.86	1.92	1.88	2.22	2.63	2.73	2.67
Tets (M)	3.50	3.02	3.14	3.10	6.39	5.06	5.26	5.16	9.14	9.66	10.03	9.87	11.46	11.48	11.89	11.61	14.14	16.25	16.85	16.51
Bad Tets	$> 0.6M$	232	201	226	$> 1.2M$	967	935	1004	$> 1.6M$	1381	1294	1375	$> 2.0M$	1746	1670	1751	$> 2.6M$	2330	2149	2380

TABLE I

EXPERIMENTAL RESULTS WITH 25K INPUT POINTS OF THE BALL DISTRIBUTION. "TETS" DENOTES TETRAHEDRA.

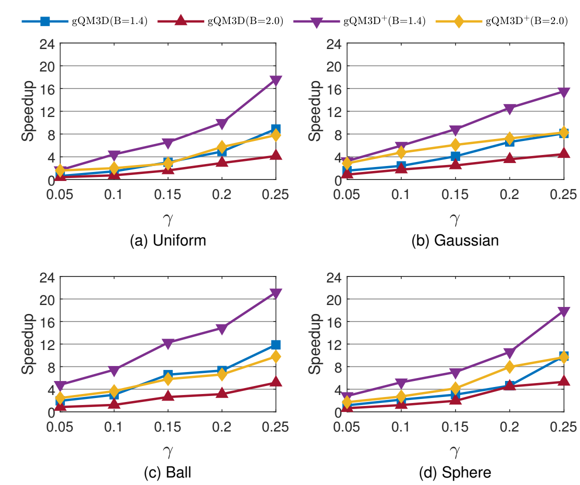

Fig. 8. Speedup of gQM3D and gQM3D$^+$ in the various distributions.

Fig. 9. Timing breakdown of gQM3D and gQM3D$^+$ in different distributions with $B = 1.4$ and $\gamma = 0.25$.

the process. We see that SplitBadTets gradually increases the performance of inserting more Steiner points but being interrupted regularly along the way, with low performance of inserting fewer Steiner points (due to Line 32 and 33). The performance then decreases towards the end of the computation with a long tail. On the other hand, SplitBadElements quickly jumps to high performance and consistently maintains high performance until it decays quickly to end the computation. This demonstrates that gQM3D$^+$ is able to maintain high utilization of GPU capacity to complete its computation as it

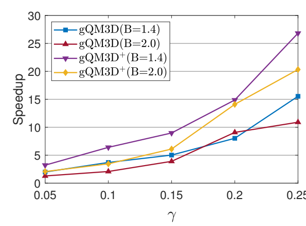

Fig. 10. The speedup of SplitBadTets and of SplitBadElements when compared to the corresponding routine in TetGen for the sphere distribution.

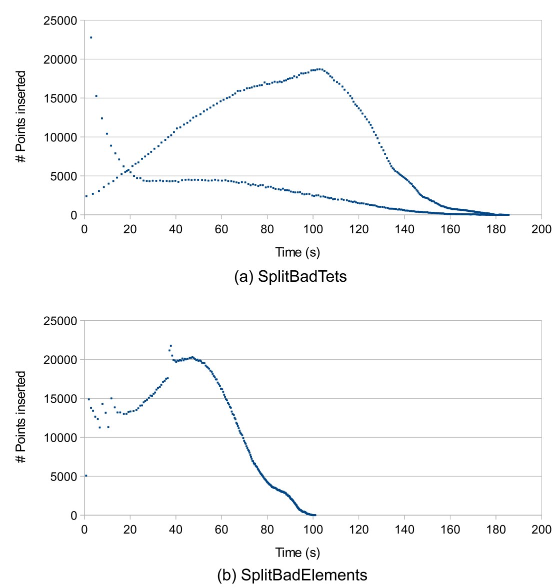

Fig. 11. General pattern of concurrency in (a) SplitBadTets and (b) SplitBadElements. This is on a sphere distribution with 20K input points, $\gamma = 0.25$, $B = 1.4$, and 4M output points.

has parallelism within the splitting of each type of elements, as well as, parallelism across different types of elements.

Output Sizes

Table I also shows the number of points in the output

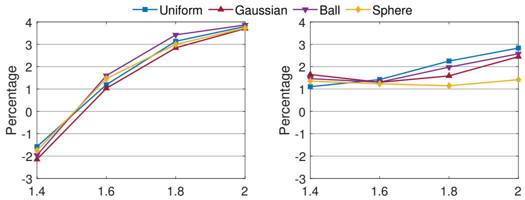

(a) gQM3D (b) gQM3D$^+$

Fig. 12. Comparison (in percentage difference) of the number of Steiner points in the output triangulations of `gQM3D`, `gQM3D`$^+$ and `TetGen` for $\gamma = 0.05$. Negative means fewer Steiner points in our software while positive means otherwise.

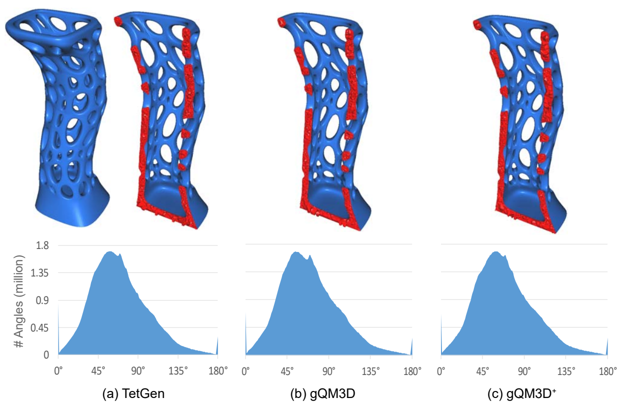

Fig. 13. The distributions of dihedral angles in the output triangulations of Sculpture as generated by the various software.

triangulation for the ball distribution and under different B by the various software. To better appreciate this, Figure 12 shows the percentage difference in the number of Steiner points in the output triangulations of `gQM3D` and `gQM3D`$^+$ as compared to that of `TetGen`. For all distributions and under different γ, their output sizes differ by at most, a small, 4%. This means that both `gQM3D` and `gQM3D`$^+$ can achieve good speedups and, at the same time, produce outputs of similar sizes. On the other hand, the difference in size seems to increase with larger B. We reckon that `gQM3D` and `gQM3D`$^+$ are aggressive in creating short edges in parallel that result in slightly more insertions of splitting points.

C. Real-world Dataset

We tested `gQM3D`, `gQM3D`$^+$ and `TetGen` on some samples from the Thingi10k dataset [29] with $B = 1.4$ and the results are shown in Table II. The speedup of `gQM3D` and `gQM3D`$^+$ over `TetGen` reached up to 19 and 34 times, respectively, while producing triangulations with similar sizes. The cut-off view and the typical distribution of dihedral angles (ranging from 0° to 180°) in the triangulations generated by them on the Model 65942, Sculpture, are shown in Figure 13. All three outputs have comparable distributions, which are also true for other real-world (and synthetic) samples we have tested on. Note that all three software generated larger numbers of bad tetrahedra in the outputs of these real-world samples as compared to those of our synthetic ones. This is because the real-world samples have a lot more small input angles which become part of those bad tetrahedra in the outputs.

Model ID Name Points Faces	Software	Points (M)	Tets (M)	Bad Tets (M)	Time (min)	Speedup
65942						
Sculpture	TetGen	4.54	20.59	1.87	71.4	1
377154	gQM3D	4.50	20.27	1.87	3.6	19.8
754688	gQM3D$^+$	4.44	20.04	1.96	2.1	34.0
63788						
Skull	TetGen	4.27	19.72	1.63	66.5	1
195452	gQM3D	4.20	19.23	1.67	3.8	17.5
392040	gQM3D$^+$	4.36	20.13	1.63	2.2	30.2
63785						
Half-skull	TetGen	3.29	15.11	1.23	39.3	1
172466	gQM3D	3.33	15.25	1.23	3.3	11.9
345996	gQM3D$^+$	3.30	15.15	1.27	1.5	26.2
94059						
Mask	TetGen	2.54	11.33	1.35	24.8	1
172466	gQM3D	2.55	11.27	1.35	2.1	11.8
345996	gQM3D$^+$	2.61	11.60	1.35	1.2	20.7
793565						
SkullBox	TetGen	2.13	9.63	0.93	17.2	1
160481	gQM3D	2.14	9.60	0.93	2.7	6.4
320978	gQM3D$^+$	2.15	9.68	0.96	1.4	12.3
252653						
Thunder	TetGen	2.93	13.60	1.04	29.5	1
239522	gQM3D	2.95	13.57	1.04	7.0	4.2
479040	gQM3D$^+$	2.99	13.85	1.04	2.8	10.5
763718						
Jacket	TetGen	1.83	8.34	0.83	12.1	1
160481	gQM3D	1.78	8.04	0.83	2.8	4.3
320978	gQM3D$^+$	1.85	8.44	0.83	1.4	8.6
1717685						
Brain	TetGen	2.98	13.53	0.90	24.6	1
396451	gQM3D	2.99	13.49	0.90	4.4	5.6
792898	gQM3D$^+$	3.02	13.78	0.90	3.4	7.2
87688						
Shy-light	TetGen	1.20	5.24	0.61	5.4	1
128216	gQM3D	1.21	5.29	0.62	4.2	1.3
256428	gQM3D$^+$	1.19	5.20	0.63	0.8	6.8
461112						
Mutant	TetGen	3.29	14.92	1.27	28.9	1
402686	gQM3D	3.39	15.28	1.27	5.4	5.4
805376	gQM3D$^+$	3.29	14.92	1.30	4.4	6.6

TABLE II
EXPERIMENTAL RESULTS ON SOME SAMPLES IN THINGI10K.

VI. CONCLUDING REMARKS

This paper proposes the first GPU algorithm for the 3D CDT refinement problem. It is designed with regularized work in mind to be GPU-friendly. In particular, the algorithm uses various lists stored as arrays in GPU global memory to linearize computations so that thousands of GPU threads can be efficient and effective in the concurrent insertions of Steiner points. Our implementations of `gQM3D` and `gQM3D`$^+$ run up to an order of magnitude faster than the `TetGen` software, and yet can produce triangulations of similar sizes and comparable qualities.

With this work, the computation of a quality triangulation can possibly be an integral part of interactive engineering or scientific applications. In addition, the strategies adapted here are of independent interest to the study of using GPU on other variants of 3D or surface triangulation problems to achieve good speedup.

REFERENCES

[1] G. L. Miller, "Control Volume Meshes Using Sphere Packing," in *Solving Irregularly Structured Problems in Parallel*, A. Ferreira, J. Rolim, H. Simon, and S.-H. Teng, Eds. Berlin, Heidelberg: Springer Berlin Heidelberg, 1998, pp. 128–131.

[2] J. R. Shewchuk, "Tetrahedral Mesh Generation by Delaunay Refinement," in *Proceedings of the Fourteenth Annual Symposium on Computational Geometry*. New York, NY, USA: ACM, 1998, pp. 86–95.

[3] H. Si, "TetGen, a Delaunay-Based Quality Tetrahedral Mesh Generator," *ACM Trans. Math. Softw.*, vol. 41, no. 2, pp. 11:1–11:36, Feb. 2015.

[4] C. Marot, J. Pellerin, and J. Remacle, "One Machine, One Minute, Three Billion Tetrahedra," *CoRR*, vol. abs/1805.08831, 2018. [Online]. Available: http://arxiv.org/abs/1805.08831

[5] P. Foteinos and N. Chrisochoides, "Dynamic Parallel 3D Delaunay Triangulation," in *Proceedings of the 20th International Meshing Roundtable*, W. R. Quadros, Ed. Berlin, Heidelberg: Springer Berlin Heidelberg, 2012, pp. 3–20.

[6] L. P. Chew, "Guaranteed-Quality Triangular Meshes," Department of Computer Science, Cornell University, Tech. Rep. 89–983, 1989.

[7] ——, "Guaranteed-Quality Mesh Generation for Curved Surfaces," in *Proceedings of the Ninth Annual Symposium on Computational Geometry*. ACM, 1993, pp. 274–280.

[8] J. Ruppert, "A Delaunay Refinement Algorithm for Quality 2-Dimensional Mesh Generation," *J. Algorithms*, vol. 18, no. 3, pp. 548–585, May 1995.

[9] Z. Chen, M. Qi, and T.-S. Tan, "Computing Delaunay Refinement Using the GPU," in *Proceedings of the 21st ACM SIGGRAPH Symposium on Interactive 3D Graphics and Games*. New York, NY, USA: ACM, 2017, pp. 11:1–11:9.

[10] T. K. Dey, C. L. Bajaj, and K. Sugihara, "On Good Triangulations in Three Dimensions," in *Proceedings of the First ACM Symposium on Solid Modeling Foundations and CAD/CAM Applications*. New York, NY, USA: ACM, 1991, pp. 431–441.

[11] L. P. Chew, "Guaranteed-Quality Delaunay Meshing in 3D (Short Version)," in *Proceedings of the Thirteenth Annual Symposium on Computational Geometry*. New York, NY, USA: ACM, 1997, pp. 391–393.

[12] J. R. Shewchuk, "Constrained Delaunay Tetrahedralizations and Provably Good Boundary Recovery," in *Eleventh International Meshing Roundtable*, 2002, pp. 193–204.

[13] H. Si, "Constrained Delaunay Tetrahedral Mesh Generation and Refinement," *Finite Elements in Analysis and Design*, vol. 46, no. 1-2, pp. 33–46, 2010.

[14] S. Oudot, L. Rineau, and M. Yvinec, "Meshing Volumes Bounded by Smooth Surfaces," in *Proceedings of the 14th International Meshing Roundtable*, B. W. Hanks, Ed. Berlin, Heidelberg: Springer Berlin Heidelberg, 2005, pp. 203–219.

[15] S.-W. Cheng, T. K. Dey, and J. A. Levine, "A Practical Delaunay Meshing Algorithm for a Large Class of Domains," in *Proceedings of the 16th International Meshing Roundtable*, M. L. Brewer and D. Marcum, Eds. Berlin, Heidelberg: Springer Berlin Heidelberg, 2008, pp. 477–494.

[16] P. Alliez, C. Jamin, L. Rineau, S. Tayeb, J. Tournois, and M. Yvinec, "3D Mesh Generation," in *CGAL User and Reference Manual*, 4.13 ed. CGAL Editorial Board, 2018. [Online]. Available: https://doc.cgal.org/4.13/Manual/packages.html#PkgMesh_3Summary

[17] Y. Hu, Q. Zhou, X. Gao, A. Jacobson, D. Zorin, and D. Panozzo, "Tetrahedral Meshing in the Wild," *ACM Trans. Graph.*, vol. 37, no. 4, pp. 60:1–60:14, Jul. 2018.

[18] D. K. Blandford, G. E. Blelloch, and C. Kadow, "Engineering a Compact Parallel Delaunay Algorithm in 3D," in *Proceedings of the Twenty-second Annual Symposium on Computational Geometry*. New York, NY, USA: ACM, 2006, pp. 292–300.

[19] A. N. Chernikov and N. P. Chrisochoides, "Three-Dimensional Delaunay Refinement for Multi-core Processors," in *Proceedings of the 22nd Annual International Conference on Supercomputing*. New York, NY, USA: ACM, 2008, pp. 214–224.

[20] P.-L. George and H. Borouchakin, *Delaunay Triangulation and Meshing: Application to Finite Elements*. Hermes Science Publications, 1998.

[21] L. Guibas and J. Stolfi, "Primitives for the Manipulation of General Subdivisions and the Computation of Voronoi Diagrams," *ACM Trans. Graph.*, vol. 4, no. 2, pp. 74–123, Apr. 1985.

[22] J. R. Shewchuk, "Triangle: Engineering a 2D Quality Mesh Generator and Delaunay Triangulator," in *Applied Computational Geometry Towards Geometric Engineering*, M. C. Lin and D. Manocha, Eds. Berlin, Heidelberg: Springer Berlin Heidelberg, 1996, pp. 203–222.

[23] B. Joe, "Three-Dimensional Triangulations from Local Transformations," *SIAM J. Sci. and Stat. Comput.*, vol. 10, no. 4, pp. 718–741, 1989.

[24] J. R. Shewchuk, "A Condition Guaranteeing the Existence of Higher-Dimensional Constrained Delaunay Triangulations," in *Proceedings of the Fourteenth Annual Symposium on Computational Geometry*, 1998, pp. 76–85.

[25] J. R. Shewchuk and H. Si, "Higher-Quality Tetrahedral Mesh Generation for Domains with Small Angles by Constrained Delaunay Refinement," in *Proceedings of the Thirtieth Annual Symposium on Computational Geometry*. New York, NY, USA: ACM, 2014, pp. 290–299.

[26] J. Nickolls, I. Buck, M. Garland, and K. Skadron, "Scalable Parallel Programming with CUDA," *Queue*, vol. 6, no. 2, pp. 40–53, Mar. 2008.

[27] J. R. Shewchuk, "Adaptive Precision Floating-Point Arithmetic and Fast Robust Geometric Predicates," *Discrete & Computational Geometry*, vol. 18, pp. 305–368, 1997.

[28] H. Edelsbrunner and E. P. Mücke, "Simulation of Simplicity: A Technique to Cope with Degenerate Cases in Geometric Algorithms," *ACM Trans. Graph.*, vol. 9, no. 1, pp. 66–104, Jan. 1990.

[29] Q. Zhou and A. Jacobson, "Thingi10K: A Dataset of 10,000 3D-Printing Models," *CoRR*, vol. abs/1605.04797, 2016. [Online]. Available: http://arxiv.org/abs/1605.04797